^{93}Nb(n,xp), ^{nat}Ag(n,xp), and ^{nat}In(n,xp) reactions at 14.1 MeV

R. Fischer, M. Uhl, and H. Vonach
Institut für Radiumforschung und Kernphysik der Universität Wien, 1090 Wien, Austria
(Received 10 August 1987)

The energy and angular distributions from the ^{93}Nb(n,xp), ^{nat}Ag(n,xp), and ^{nat}In(n,xp) reactions were investigated by means of a multitelescope system. Targets, thick compared to the range of the most energetic protons, were used and the double-differential proton emission cross sections were derived by unfolding. The results for both the angle-integrated proton spectra and the proton energy dependence of the angular distributions are very similar for all three measured cases and confirm that the (n,p) reaction at 14 MeV is dominated by precompound emission in the studied mass range. The angle-integrated results are compared with calculations based on the statistical model of nuclear reactions including both precompound particle emission and subsequent particle evaportation. It is shown that the proton spectra can be adequately described within this model, if the usual pairing correction for level densities is also applied to the exciton state densities used in the calculation of precompound particle emission and the matrix element for internal transitions is chosen in such a way that the rate of $3\rightarrow 5$ exciton transitions is adjusted to 5×10^{21} sec^{-1}. With this choice of parameters it is simultaneously possible to describe the neutron spectra in the ^{93}Nb(n,n') reaction except at the highest energies where an additional direct reaction component is required. The angular distribution which show a strongly energy dependent forward-backward asymmetry are in fair agreement with the phenomenological model of Kalbach-Mann and with those of direct reaction theory for continuum cross sections.

I. INTRODUCTION

Our program of investigations of (n,p) reactions[1] at $E_n = 14.1$ MeV was continued with the ^{nat}Ag(n,xp) and ^{nat}In(n,xp) reactions. These reactions were selected to supplement our (n,p) measurements[1] in order to study the systematic behavior of the angular distributions of the emitted protons in the mass region around $A = 100$, where up to now no other detailed measurements of such angular distributions exist.

As we especially wanted to study angular distributions in precompound proton emission, targets thick compared to the range of the most energetic protons, were used and the double-differential particle emission spectra were subsequently derived by unfolding the thick target spectra.

In this way it is possible to measure the high energy parts of the spectra with much better accuracy in a given measuring time than with the conventional thin target method, and, also, the results are much less sensitive to the background since the use of thick targets greatly enhances the measuring effect compared to the background. In order to demonstrate the validity of this method we also performed a thick target measurement of the ^{93}Nb(n,p) reaction, which had been studied before in the conventional way.[1] In this way we also considerably improved the accuracy of the ^{93}Nb data for the high proton energies. Thus we will also report improved data on the ^{93}Nb(n,p) reaction obtained from combining the results of Ref. 1 and those of the new thick target measurements.

II. EXPERIMENTAL PROCEDURE

The (n,p) reactions were studied by means of a multitelescope system irradiated by 14.1 MeV neutrons produced in the 250 keV accelerator of the Institut für Radiumforschung und Kernphysik. As the multitelescope system has been described before,[2,3] only a few details that are specific to this experiment are given.

All targets used were thick compared to the range of the most energetic (14.7 MeV) protons. Metallic silver and niobium sheets ~ 0.7 mm thick and indium sheets 1 mm thick were used. As the background in these thick target measurements amounts to only a few percent, the whole reaction chamber (all 32 telescopes) was used for the measurements with the various targets and the background was determined in a separate shorter background run with a thick gold target in place of the target foils. The background, measured in this way, is an overestimate of the background, as a larger part of the gold surface seen by the telescopes in the background measurement is shielded by the targets in the effect measurement (see Fig. 3 of Ref. 2). This effect was calculated from the geometry used and accordingly the actual background was assumed to be only 32% of the result of the background run.

Since this background correction was between 8 and 20% for all reactions investigated, the uncertainty from this procedure is quite small.

Each of the targets was irradiated for about 100 h at a neutron source strength of $\sim 2.2\times 10^9$ nsec resulting in a maximum neutron flux of 1.2×10^5 n/cm^2 sec at the tar-

get position.

The integral neutron flux was determined by two independent methods, a LiI scintillator monitor placed in the shielding of the accelerator room and ^{59}Co(n,2n)^{58}Co activation monitors at the actual position of the multitelescope system as described before.[4] Both methods agreed within 3%.

In order to improve the accuracy of the p-energy calibration, two of the 32 telescopes were used for an energy calibration during the actual experiments. One of the telescopes (at 24°) was equipped with a polyethylene foil (2.89 mg/cm^2) and observation of the recoil proton peak provided a calibration point of about 12 MeV; another one was used to observe 5 MeV α particles from a ^{241}Am source. In this way the p-energy scale could be established to better than 200 keV at 14 MeV and even more accurate at lower energies.

III. DATA ANALYSIS

By selecting appropriate areas in the energy-energy loss and energy-pulse-shape planes, thick target proton energy spectra were obtained for 16 reaction angles ranging from 22° to 165°. The angular resolution of the telescopes was on average 13°. The total number of true events turned out to be ~230 000 for Ag, ~90 000 for In, and ~180 000 for Nb. To obtain the p-emission spectra the measured "thick target" spectra $N(E_p)$ had to be unfolded. This was done by numerically differentiating the quantity $(dE_p/dx)\cdot N(E_p)$ with respect to E_p (dE_p/dx=specific energy loss for protons of energy E_p). Given in detail, the following simple procedure was used. After subtraction of background each spectrum $N(E_p)$ channel by channel was multiplied by the specific energy loss $(dE_p/dx)(E_I)$ (Ref. 5) (E_I=energy of channel I) and the resulting spectrum

$$\bar{N}(E_I)=N(E_I)(dE/dx)(E_I)$$

was differentiated by calculating

$$N'(E_I)=[\bar{N}(E_{I+1})-\bar{N}(E_{I-1})]/(E_{I+1}-E_{I-1}) ,$$

giving the equivalent thin target spectrum $N'(E_I)$, out of which the differential cross section could be calculated in the usual way.

In the measurement the proton energy spectrum was recorded with a channel width of ~90 keV, for the described analysis the spectra were collapsed by a factor of 5 resulting in a channel width of ~450 keV. Thus the differentiated values $N'(E_I)$ are essentially averaged over 0.9 MeV bins.

Only the calculation of the statistical errors of the double-differential particle emission had to be modified slightly. The statistical errors of the $N'(E_I)$ values can be calculated in the conventional way. In the further process of binning the data into the usual 1 MeV bins, however, the correlations between $N'(I)$ and its second neighbors $N'(I-2)$ and $N'(I+2)$ would lead to an overestimate of the statistical error. This way was taken into account by an approximate correction factor.

Figure 1 shows a typical example for the transformation of a measured thick target spectrum into an equivalent thin one. Figure 1(a) is the measured thick target spectrum, (b) is the thick target spectrum multiplied by $(dE/dx)E_I$ and (c) is the transformed spectrum derived by numerical differentiation of (b).

A comparison of p-emission spectra of the two ^{93}Nb experiments is shown in Fig. 2. The data of both experiments agree within the 1σ error bars. At the high energy end, the accuracy of the thick target data is superior to the thin target data, *vice versa,* it is at the low energy end. In the comparison of the two data sets it has to be taken into account that the thin target data needed about 3 times more measuring time than the thick target data.

IV. EXPERIMENTAL RESULTS AND COMPARISON WITH EARLIER MEASUREMENTS

The data obtained by the procedure described above represent the double differential p-emission cross section determined at 16 reaction angles ranging from 24° to 164° with a typical resolution of 13°; the energy resolution is assumed to be better than ~1.5 MeV. For further discussion and comparison with the results of other authors, it is useful to integrate over either angle or energy: angle integrated p-emission cross sections for 1 MeV en-

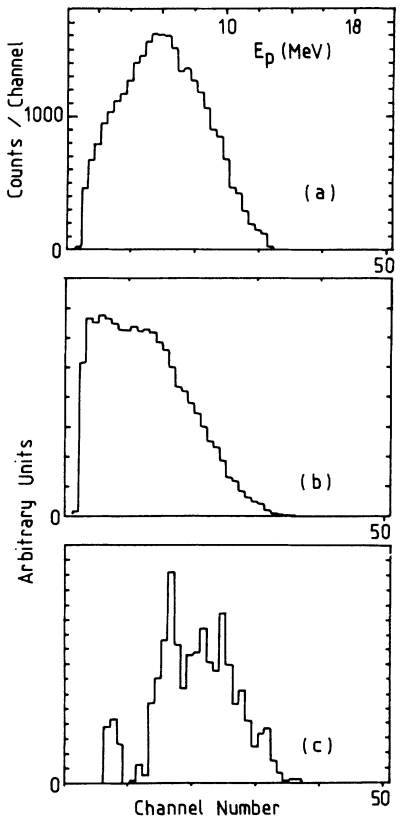

FIG. 1. Typical data from thick target experiment. (a) Proton spectra for thick Nb target at $\theta=22°$; (b) same multiplied by $dE_p/dx(E_p)$; (c) equivalent thin target spectrum obtained by numerical differentiation of (b).

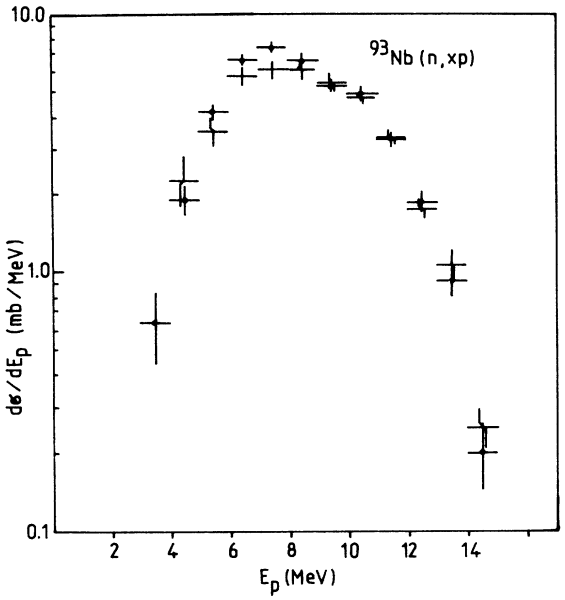

FIG. 2. Comparison of the angle integrated proton emission cross sections from the ^{93}Nb(n,xp) reaction at $E_n = 14.1$ MeV from different experiments. E_p represents the channel energy. ● represents the thin target experiment (10 mg/cm^2), 220 h measuring time, and ○ represents the thick target experiment ($\sim$0.7 g/cm^2), 75 h measuring time.

ergy bins were obtained by Legendre fits to the $(d^2\sigma)/(dE_p d\theta)$ values. The numerical values for these angle integrated p-emission cross sections are listed in Table I together with the corresponding 1σ errors combining both statistical and all identified systematic error contributions [essentially, uncertainties in the neutron flux (3%) and in the solid angle of the central detector (2%), error in the dE/dx values (3%), and errors due to the data reduction procedure (2%)]. For niobium the weighted average of the results of this work and our previous thin target experiment[1] is given.

The total proton emission cross sections amount to 42.4±2 mb for ^{93}Nb, 31.4±1.5 mb for ^{nat}Ag, and 12.6±0.6 mb for ^{nat}In.

The angular distributions of the protons (see Figs. 11 and 12) are forward peaked for all but the very lowest energies; the amount of the forward-backward asymmetry increases strongly with proton energy. For all energies, however, the angular distributions can be well described by a series of Legendre polynomials up to $l=2$. Thus the information on the angular distributions can be summarized in form of the reduced Legendre coefficients $a_1/a_0(E_p)$ and $a_2/a_0(E_p)$ derived from least squares fits of the form

$$\frac{d^2\sigma}{dE_p d\Omega} = \sum_{l=0}^{2} a_l P_l(\cos\theta)$$

which are given in Table II.

Again for Nb the weighted average of the results of this experiment and our previous thin target measurements is given.

The given uncertainties of the reduced Legendre coefficients were also determined from the least squares fits.

Concerning the comparison with previous measurements we refer to Ref. 1 for the ^{93}Nb(n,xp) reaction, as the addition of our new results (see Fig. 2) caused only minor changes.

For the ^{nat}Ag and ^{nat}In there exists one measurement of the proton emission spectrum in the forward direction (0°–15°) using a counter telescope.[6] For indium there exist, in addition the counter telescope, results of Niidome *et al.*[7] (reporting both angle integrated proton spectra and the energy integrated proton angular distribution) and of Hans and Mohindra[8] (reporting proton spectra at angles in the range 0°–135°) and one nuclear emulsion study[9] of proton emission in the forward direction (0°–37°). The emulsion study disagrees completely with all other experiments and shows some rather strange structure, thus it will not be discussed further.

Our data agree (within the rather large experimental errors) with the results of Ref. 7, as shown in Figs. 3 and

TABLE I. Angle-integrated proton emission cross sections at $E_n = 14.1$ MeV.

	$d\sigma/d\Omega$ (mb/MeV)		
E_p (MeV)	^{93}Nb	^{nat}Ag	^{nat}In
2–3	0.64±0.18		
3–4	1.98±0.30	0.75±0.38	
4–5	3.97±0.35	1.14±0.35	0.29±0.29
5–6	6.27±0.45	3.86±0.37	1.51±0.27
6–7	6.77±0.65	5.08±0.37	1.50±0.24
7–8	6.38±0.40	4.99±0.35	2.04±0.23
8–9	5.35±0.35	4.53±0.30	2.75±0.23
9–10	4.82±0.35	4.07±0.26	2.30±0.19
10–11	3.30±0.30	3.33±0.21	1.32±0.13
11–12	1.78±0.15	2.02±0.14	0.56±0.08
12–13	1.00±0.08	1.04±0.07	0.28±0.05
13–14	0.24±0.06	0.44±0.05	0.09±0.03
14–15		0.17±0.02	

TABLE II. Reduced Legendre coefficients describing the angular distributions of the protons from the (n,p) reactions on ^{93}Nb, ^{nat}Ag, and ^{nat}In.

	^{93}Nb	^{nat}Ag	^{nat}In
E_p (MeV)	a_1/a_0	a_1/a_0	a_1/a_0
4–6	0.19±0.09	0.12±0.10	0.12±0.23
6–8	0.44±0.03	0.31±0.04	0.62±0.10
8–10	0.70±0.03	0.72±0.04	0.85±0.05
10–12	0.85±0.035	0.93±0.04	1.05±0.08
12–14	0.86±0.09	0.97±0.06	1.15±0.12
	a_2/a_0	a_2/a_0	a_2/a_0
4–6	0.08±0.08	0.04±0.15	
6–8	0.28±0.04	0.16±0.09	0.32±0.13
8–10	0.30±0.04	0.33±0.05	0.40±0.07
10–12	0.34±0.04	0.40±0.05	0.48±0.11
12–14	0.38±0.08	0.42±0.08	0.70±0.25

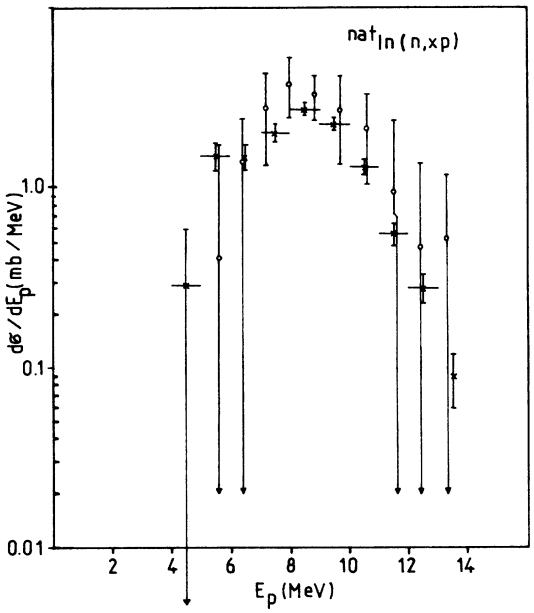

FIG. 3. Comparison of our angle integrated proton emission spectra from the reaction ^{nat}In(n,xp) with those of Ref. 7. × represents the present result and ○ represents the result of Ref. 7.

4, both with respect to the proton energy and angular distributions; also the total proton emission cross section 18.1±5.4 mb from Ref. 7 is consistent with our result of 12.6±0.6 mb.

There are, however, considerable discrepancies between our data and the results of the earlier telescope work of Refs. 6 and 8. As shown in Figs. 5 and 6, both the form of the angular distribution in Ref. 8 and the energy spectra in forward direction from Refs. 6 and 8 deviate considerably from our results.

No obvious reasons for these discrepancies can be suggested; very little information on the experimental details is given in either Ref. 6 or 8; thus one can only speculate that problems associated with either the background subtraction or the rather large target thickness ($\sim$30 mg/cm^2) might have influenced the earlier data.

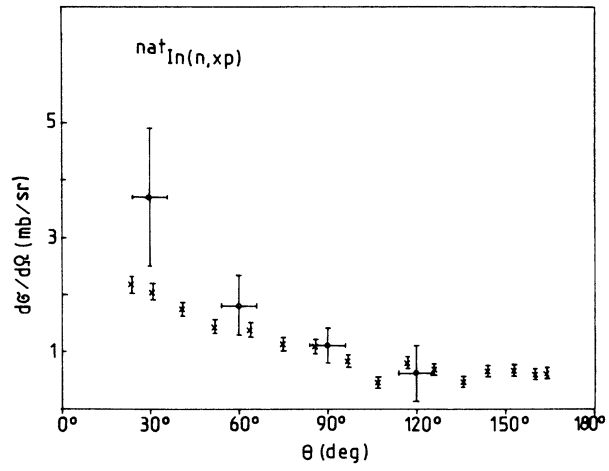

FIG. 4. Comparison of our proton angular distributions for the ^{nat}In(n,xp) reaction with the results of Ref. 7. × represents the present result and ○ represents the result of Ref. 7.

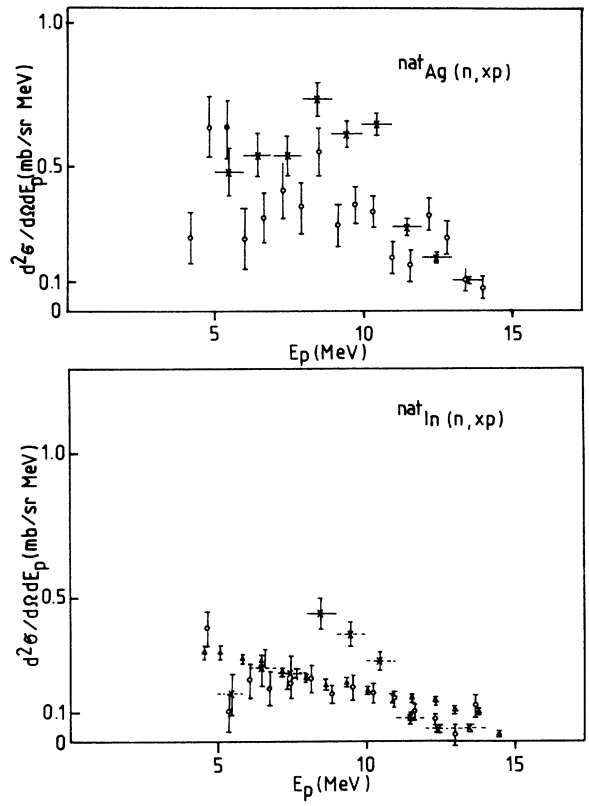

FIG. 5. Comparison of the proton emission spectra from the ^{nat}Ag(n,xp) and ^{nat}In(n,xp) reactions in forward direction with earlier measurements. × represents the result [average of telescope 1 (24°) and telescope 2 (31°)], ○ represents the result of Ref. 6 and △ represents the result of Ref. 8.

In addition, there have been a number of activation measurements of the (n,p) cross sections of ^{107}Ag, ^{109}Ag, and ^{115}In; however, in all cases the reactions feed two isomers, and measurements to one isomer in ^{115}Cd and to one in ^{107}Pd are missing. Thus no direct comparison of these activation cross sections with our proton emission cross sections is possible.

V. COMPARISON WITH THEORY

A. Angle-integrated cross sections

Proton emission in nuclear reactions in the studied mass and energy range is due to both precompound emission and particle evaporation from fully equilibrated compound nuclei with comparable contributions from both processes.[1] Accordingly the experimental results were compared to nuclear model calculations using the exciton model for precompound particle emission and the Hauser-Feshbach theory for the compound nucleus decay using the code MAURINA.[10] The main ingredients of the exciton model calculations were internal transition

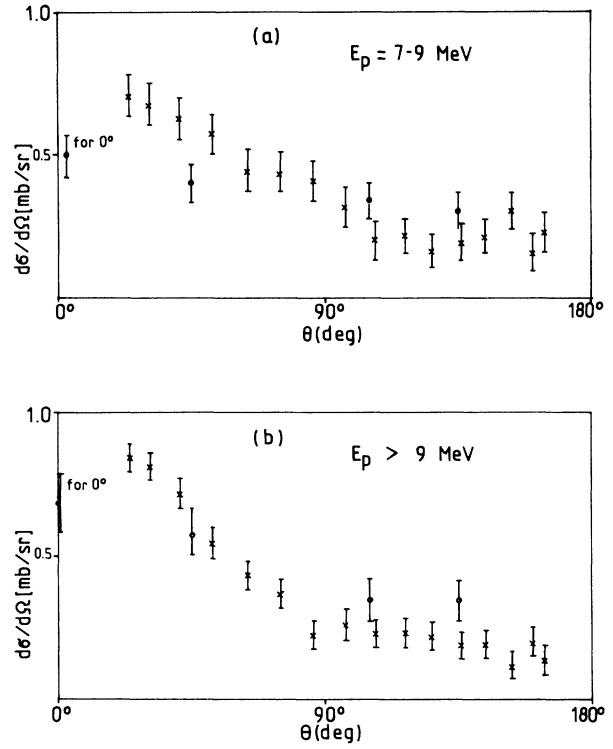

FIG. 6. Comparison of our angular distributions for the ^{nat}In(n,xp) reaction with the results of Ref. 8. (a) $E_p = 7-9$ MeV; (b) $E_p > 9$ MeV. × represents the present results and ○ represents the Hans and Mohindra (Ref. 8).

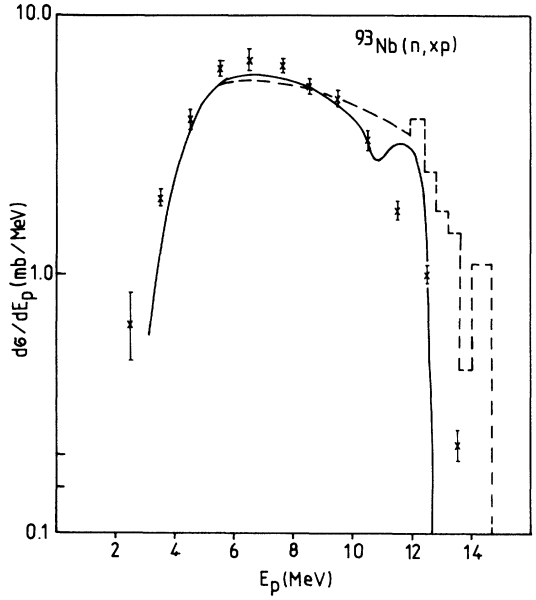

FIG. 7. Comparison of the angle-integrated proton spectrum from the reaction ^{93}Nb(n,xp) with nuclear model calculations. × represents the experimental cross sections, the solid curve —— represents the calculation with parameters of Table III, and the dashed curve — — — represents the calculation without pairing correction for excition states and with FM changed to 700 MeV[3].

rates according to Oblozinsky *et al.*,[11] detailed balance based particle emission rates which account for neutron-proton distinguishability as proposed by Gadioli *et al.*,[12] and William's formula[13] for the particle hole state density of the residual nuclei. Figures 7–10 show the results obtained with the parameters listed in Table III. The calculation of the compound nucleus part is very sensitive to the level density parameters of the residual nuclei populated by proton and neutron emission and to the (n,p) Q value and the results may be very different even for neighboring nuclei. Thus the equilibrium part of the calculation was fitted individually to the low energy parts of the measured spectra by adjusting the mentioned level density parameters. This was possible in all cases within the known uncertainties of these level density values.

Precompound particle emission, on the other hand, is rather insensitive to the properties of individual nuclei and if a phenomenological model like the exciton model is a good approximation at all it should not need individual parameter adjustment and also simultaneously describe precompound neutron emission, that is the high energy parts of the neutron spectra. Therefore a common set of parameters was chosen for the exciton model for all cases: density of single particle states $g = A/13.16$ (MeV^{-1}) and pairing $\Delta = A/\sqrt{12}$ (MeV) for calculation of the exciton state densities and matrix elements for internal transitions (FM values of Table III) chosen in such a way that the internal transition rates were adjusted to 5×10^{21} sec^{-1} for the first equilibration step (transition of $3\rightarrow5$ excition states).

As the figures show, there is a reasonable overall agreement between measured and calculated cross sections, both in absolute magnitude and shape also in the

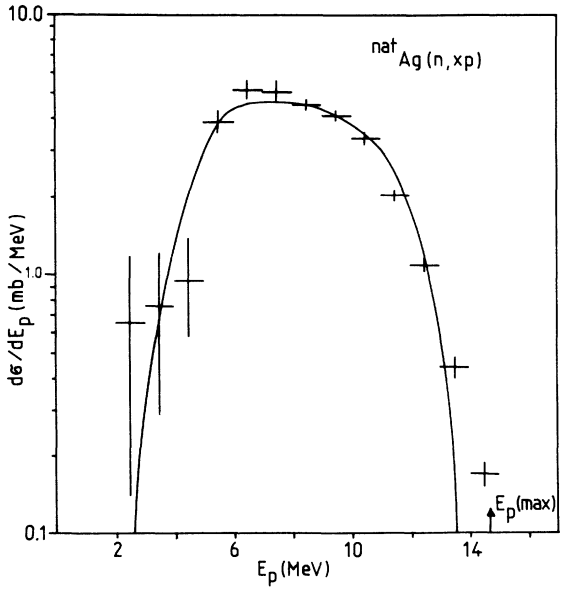

FIG. 8. Comparison of the angle-integrated proton spectrum from the reaction ^{nat}Ag(n,xp) with nuclear model calculations. The meanings of the symbols are the same as in Fig. 7.

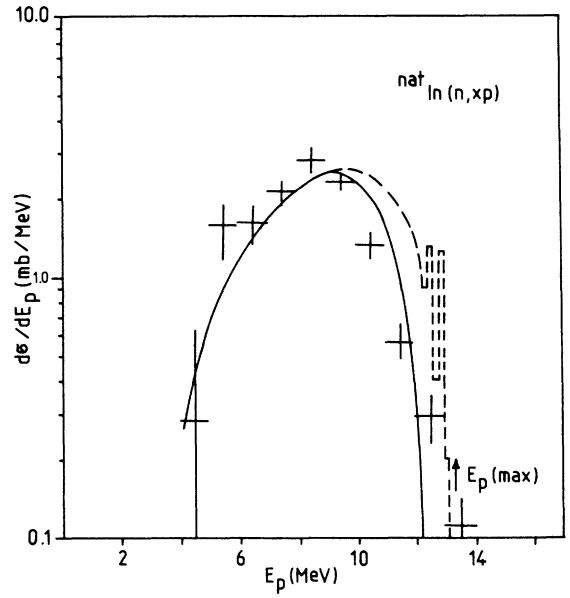

FIG. 9. Comparison of the angle integrated proton spectrum from the reaction ^{nat}In(n,xp) with nuclear model calculations. The meanings of the symbols are the same as in Fig. 7.

upper halves of the proton spectra which are dominated by precompound emission. The absolute values of the peak cross sections for proton emission is essentially determined by the value of the internal transition rates whereas the shape of the high energy part of the proton spectra depends essentially only on the chosen pairing

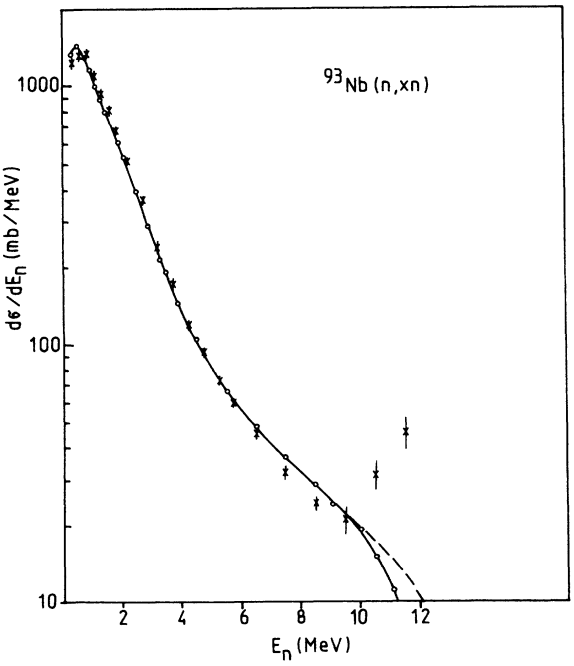

FIG. 10. Comparison of the angle-integrated neutron spectrum from the reaction ^{93}Nb(n,xn) with nuclear model calculations. The meanings of the symbols are the same as in Fig. 7.

TABLE III. Parameters FM for the internal transition matrix element ($|M|^2 = FM \cdot U^{-3} \cdot A^{+1}$) used in the model calculation.

Target nucleus	FM (MeV^3)	$\lambda(3 \rightarrow 5)$ (10^{21} sec^{-1})
^{93}Nb	420	4.7
^{107}Ag	460	4.7
^{109}Ag	460	4.6
^{115}In	470	5.1

correction for the exciton states. Thus our results imply:

(1) The internal transition rates ($3 \rightarrow 5$ exciton states) are found to be about $(5 \pm 1) \times 10^{21}$ sec^{-1}.

(2) As already pointed out in Ref. 1, there is definitely need for a pairing correction of about the usual value $\Delta = A/\sqrt{12}$ (MeV) in exciton state densities. Without such a correction (see Figs. 7 and 9) the emission of high-energy protons is greatly overestimated. It has to be noted, however, that even in applying such a correction, the shape of the spectra cannot be described perfectly. In two of the reactions studied (on ^{93}Nb and ^{nat}In) the calculated slopes of the high energy parts of the proton spectra are definitely different from the measured value. This discrepancy cannot be removed by any simple parameter variation and seems to indicate the limits of validity of the model.

Another important question, the quality of the simultaneous description of proton and neutron precompound emission, can also be tested with our data, as for one of the nuclei ^{93}Nb a rather accurate neutron emission spectrum is available from a recent evaluation of one of the authors.[14] Figure 10 shows these spectra and the results of the model calculations using the same parameters (see Table III) as for the ^{93}Nb(n,xp) spectra. As the figure shows there is good agreement up to a neutron energy of about 10 MeV, above this energy the measured neutron emission cross sections are much larger than the calculated ones, indicating that for neutron energies above ~ 10 MeV—that is, excitation energy below ~ 4 MeV—direct reactions, e.g., excitation of collective states, have to be assumed in addition to precompound neutron emission. Looking only at the neutron spectrum, exciton model calculation without pairing correction or calculations using the geometry-dependent hybrid model[15] would improve the fit to the data, and, however, at the same time produce unacceptable proton spectra (see Figs. 7 and 9).

Thus for a complete description of the interaction of 14 MeV neutrons with nuclei it seems necessary to use three reaction mechanisms (direct, precompound, evaporation) for the inelastic neutron scattering, whereas the (n,p) process does not show such direct contributions and can be better used to extract the model parameter for precompound emission.

Finally it should be remarked that the ratio between precompound proton and neutron emission for neutron energies below 10 MeV is quite well described by the form of the exciton model (using the method described in Ref. 12) in order to distinguish between neutron and proton emission) implemented in our code.

B. Angular distribution

As in Ref. 1 we will compare, in the following, the experimental results to the systematics of reduced Legendre coefficients and to the results of the one-step version of the direct reaction theory for continuum cross sections.

1. Systematics of reduced Legendre coefficients

In Ref. 1 we compared our angular distribution with a slightly modified version of the Kalbach-Mann model.[16] Essentially we replaced the division of the cross sections into a multistep direct and a multistep compound part by the conventional division into a preequilibrium and an equilibrium part; that is, we assumed that the angular distributions proposed in Ref. 15 for multistep direct reactions are also approximately valid for all precompound particles and the angular distributions for the multistep compound reaction can be used for the evaporation part. This latter assumption, however, is not necessary as the angular distribution of the evaporated particles can be calculated by the standard Hauser-Feshbach theory. Also the angular distributions suggested in Ref. 16 do not have the right asymptotic behavior; for low energies of the emitted particles the angular distributions do not approach isotropy. Thus, as modification of the Kalbach-Mann systematics, which should be especially suited for description of the angular distributions down to very low particle energies, we assumed the following:

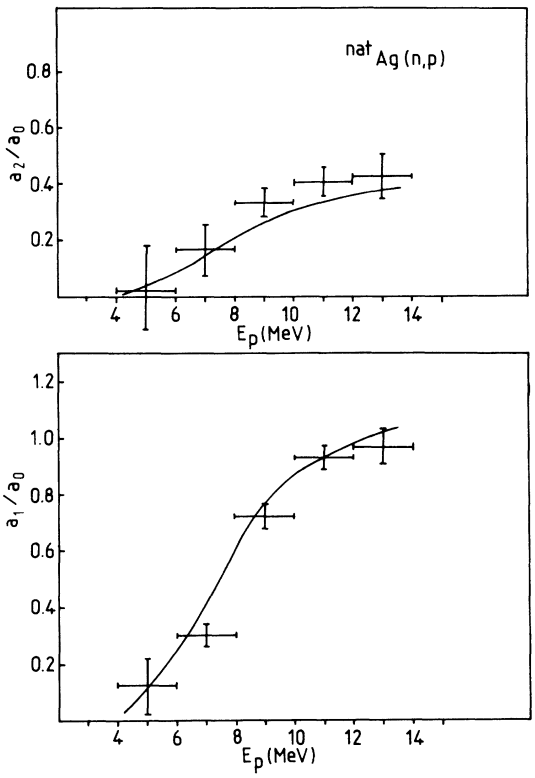

FIG. 12. Reduced Legendre coefficients for the ^{nat}Ag(n,xp) reaction (see the caption of Fig. 11).

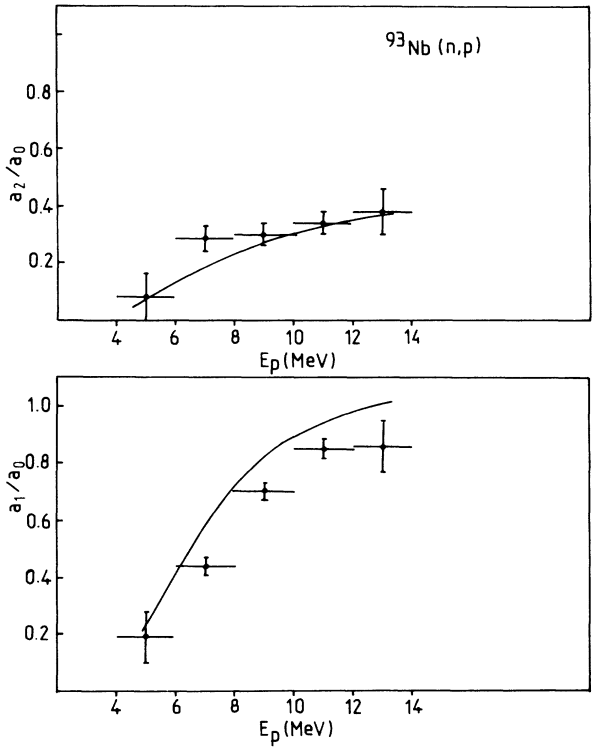

FIG. 11. Comparison of the reduced Legendre coefficients describing the angular distributions of the protons from the ^{93}Nb(n,xp) reaction with the predictions of the modified Kalbach-Mann systematics.

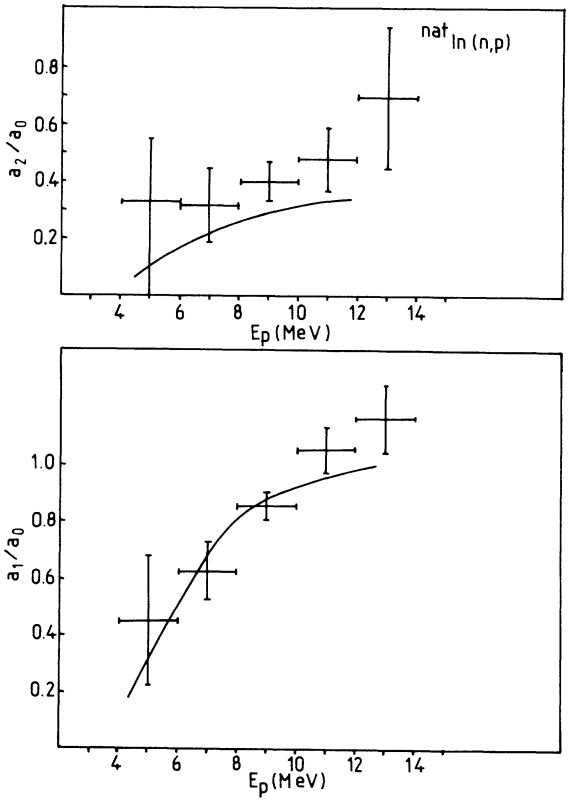

FIG. 13. Reduced Legendre coefficients for the ^{nat}In(n,xp) reaction (see the caption of Fig. 11).

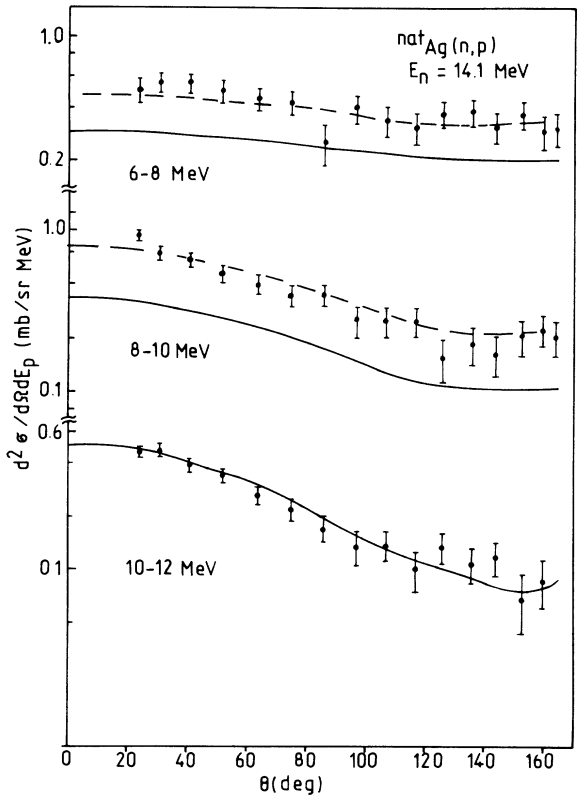

FIG. 14. Comparison of the double-differential proton emission cross sections for the ^{nat}Ag(n,xp) reaction with the predictions of the direct reaction theory of continuum cross sections.

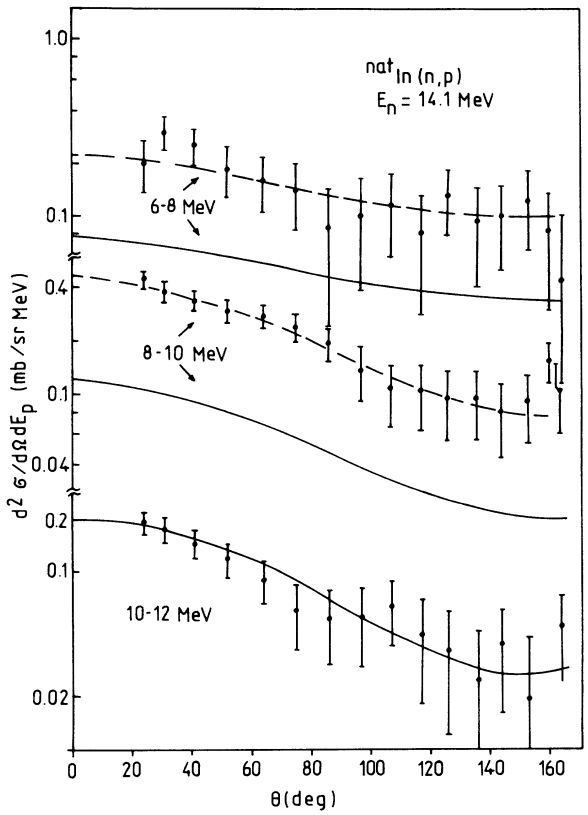

FIG. 15. Comparison of the double-differential proton emission cross sections for the ^{nat}In(n,xp) reaction with the predictions of the direct reaction theory of continuum cross sections.

(1) For the precompound particles we assumed an angular distribution exactly as given in Eqs. (2)–(5b) of Ref. 16 for multistep direct reactions.

(2) For the equilibrium part the angular distribution is calculated by means of the standard Hauser-Feshbach theory. In the present case the resulting anisotropy amounts to a few percent.

The reduced Legendre coefficients calculated in this way are compared to the experimental data of Table II and Figs. 11–13. As the figures show, the agreement is quite satisfactory in all three cases, especially considering the extreme simplicity of the model. This also means that the angular distributions of the precompound particles are equal within experimental error for all systems studied and only dependent on the particle energy.

2. *One step version of direct reaction theory for continuum cross sections*

Calculations of double differential cross sections for the reactions ^{nat}Ag(n,xp) and ^{nat}In(n,xp) were performed by means of the code ORION-TRISTAR-1.[17] More details are described in connection with an analogous comparison of our previous ^{93}Nb(n,xp) data.[1]

Figures 14 and 15, respectively, display, for ^{nat}Ag and ^{nat}In as targets, experimental and calculated cross sections for three groups of energy of the emitted protons. Besides the direct component, the calculated cross sections also include a Hauser-Feshbach contribution. For the direct continuum cross sections, the form factors $f_l(r)$ for orbital angular momentum transfer l were related to the derivative of the optical potential $U(r)$ by $f_l(r)=\beta_l(dU/dR)$. Optical potentials for protons and neutrons were chosen according to Becchetti and Greenlees.[18] The shape of the angular distributions could be reproduced by assuming the same value $\beta_l=\beta$ for all considered orbital angular momentum transfers l from 0 to 10. The solid curves in Figs. 14 and 15 were obtained with parameters β ($\beta=0.90$ for ^{nat}Ag and $\beta=0.56$ for ^{nat}In) adjusted so as to reproduce the highest energy group centered at 11 MeV, where the Hauser-Feshbach contribution is negligible. The dashed curves are normalized to the data of the two groups with lower proton energy in order to illustrate that the shapes of the angular distributions are reasonably well reproduced though the absolute cross sections are by far too small. We obtained very similar results when using for the protons the optical potential by Menet *et al.*[19] instead of that by Becchetti and Greenlees.[18]

Thus the results of this comparison for ^{nat}Ag(n,xp) and ^{nat}In(n,xp) show similar features as for ^{93}Nb(n,xp):[1] a fair reproduction of the shape of the angular distributions but difficulties in reproducing absolute cross sections for different emission energies with one set of model parameters.

[1]G. Traxler, A. Chalupka, R. Fischer, B. Strohmaier, M. Uhl, and H. Vonach, Nucl. Sci. Eng. **90**, 174 (1985).
[2]C. Derndorfer, R. Fischer, P. Hille, G. Stengl, and H. Vonach, Nucl. Instrum. Methods **187**, 423 (1981).
[3]G. Traxler, R. Fischer, and H. Vonach, Nucl. Instrum. Methods **217**, 121 (1983).
[4]R. Fischer, G. Traxler, M. Uhl, H. Vonach, and P. Maier-Komor, Phys. Rev. C **34**, 460 (1986).
[5]H. H. Andersen and J. F. Ziegler, *Hydrogen Stopping Powers and Ranges in All Elements* (Pergamon, New York, 1977).
[6]H. P. Eubank, R. A. Peck, Jr., and M. R. Zatzick, Nucl. Phys. **10**, 418 (1959).
[7]J. Niidome *et al.*, Nucl. Phys. **A245**, 509 (1975).
[8]H. S. Hans and R. K. Mohindra, Nucl. Phys. **47**, 473 (1963).
[9]R. A. Peck, Phys. Rev. **123**, 1738 (1961).
[10]M. Uhl (unpublished).
[11]P. Oblozinskỳ, I. Ribansky, and E. Beták, Nucl. Phys. **A226**, 347 (1974).
[12]E. Gadioli-Erba and P. G. Sona, Nucl. Phys. **A217**, 589 (1973).
[13]F. C. Williams, Jr., Nucl. Phys. **A166**, 231 (1971).
[14]A. Pavlik and H. Vonach, Phys. Data (in press).
[15]M. Blann, Phys. Rev. Lett. **28**, 757 (1972).
[16]C. Kalbach and F. Mann, Phys. Rev. C **23**, 112 (1981).
[17]T. Tamura, T. Udagawa, and M. Benhamou, Comput. Phys. Commun. **29**, 391 (1983).
[18]F. D. Becchetti and G. W. Greenlees, Phys. Rev. **182**, 1190 (1969).
[19]J. J. H. Menet, E. E. Gross, J. J. Malafari, and A. Zucker, Phys. Rev. C **4**, 1114 (1971).